Directional derivative-based method for quasi-stationary voltage support analysis of single-infeed VSC-HVDC units

Perilla , Arcadio; Rueda Torres, José Luis; Rakhshani, Elyas; Irnawan, Roni; Faria da Silva, Filipe; van der Meijden, Mart; Bak, Claus Leth; Alefragkis, Alex; Lindefelt, Anna

DOI
10.1049/hve.2019.0420

Publication date
2020

Document Version
Final published version

Published in
High Voltage

High Voltage

Special Issue: Advances in High Voltage DC Systems/Grids Control, Operation, and Protection

IET Journals
The Institution of Engineering and Technology

Directional derivative-based method for quasi-stationary voltage support analysis of single-infeed VSC-HVDC units

eISSN 2397-7264
Received on 30th December 2019
Revised 9th March 2020
Accepted on 1st April 2020
E-First on 10th June 2020
doi: 10.1049/hve.2019.0420
www.ietdl.org

Arcadio Perilla[1] ✉, Jose Luis Rueda Torres[1], Elyas Rakhshani[1], Roni Irnawan[2], Filipe Faria da Silva[2], Mart van der Meijden[1,3], Claus Leth Bak[2], Alex Alefragkis[3], Anna Lindefelt[4]

[1]*Electrical Sustainable Energy Department, Delft University of Technology, Mekelweg 4, 2628 CD, Delft, The Netherlands*
[2]*Department of Energy Technology, Aalborg University, Pontoppidanstraede 111, 9220, Aalborg, Denmark*
[3]*TenneT TSO B.V, Arnhem, The Netherlands*
[4]*Energinet, Fredericia, Denmark*
✉ *E-mail: a.perilla@tudelft.nl*

Abstract: This study presents an investigation of the impact of the quasi-stationary voltage support provided by a voltage source converter (VSC) connected to a single point of a power system. Based on the directional derivative concept, an analytical method is developed to quantify the sensitivities of the AC bus voltage with respect to the VSC reactive power control modes. Based on a real case study, it is shown that the method applies to VSC units that are part of VSC-HVDC systems, which can operate in a point-to-point or multi-terminal configuration. Time-domain simulations are performed to verify the findings from the application of the analytical method on a reduced size power system.

1 Introduction

The societal ambition for acceleration in the energy transition in different places around the world is causing major technological upgrades in the electrical power systems. Within this energy transition, the role of the high voltage DC (HVDC) systems is becoming highly relevant for the power system stability analysis. This is especially true in Europe, where, since the last decade, the amount of new HVDC projects connected to the transmission network has been considerably increased [1–3]. All of these new HVDC projects (which are mostly based on voltage source converter (VSC) units) have design considerations to provide certain levels of reactive power, which can be used to improve the voltage profile in the transmission networks. This is in line with other reported applications of VSC units for controlled series or parallel reactive power compensation (e.g. STATCOM or FACTS devices in [4, 5]).

The voltage stability (VS) analysis utilising VSC-HVDC links has been so far tackled by using two main methodologies. On the one hand, some works have focused on the assessment and adjustment of the voltage's profile and reactive power control (RPC) of the VSC-HVDC links by using the power flow Jacobian method [6, 7]. On the other hand, some works have used the PV curve analysis method [8, 9] to study the VS considering the effect of limiting the current provided by the VSC-HVDC system or by assessing its performance, during weak network conditions. Other research works have tackled the VS problem by performing time-domain simulations in which the implications of a simultaneous voltage regulation scheme for VSC-HVDC systems and other voltage support units are analysed. For instance in [10], it is indicated that the deployment of the reactive power reserve of a VSC-HVDC system combined with the automatic voltage regulator (AVR) actions can maintain the network voltage's profile within acceptable ranges. However, in [11], it is pointed out that the parameters (time constants) of the RPC modes need to be chosen forestalling the control actions of other AC voltage regulation devices (i.e. on load transformer taps changers).

Moreover, due to the significant reduction of the short-circuit power levels in the power system (caused by the phase-out of conventional power plants), there are major concerns regarding the influence of the RPC modes that can be used for VS support. For instance, in the design considerations of one of the most recent and fully operational VSC-HVDC European project, i.e. the COBRAcable project [12], and in compliance with the European HVDC grid code [13], it is established that any VSC-HVDC unit should be capable of providing voltage support by using at least one of the followings RPC modes: the AC voltage control (U_{ACCtrl}) mode, the RPC (Q_{Ctrl}) mode, and the power factor control ($\mathrm{PF}_{\mathrm{Ctrl}}$) mode. Thus, the selection of the RPC modes for the operation of a VSC-HVDC system constitutes an important aspect in the study of the impact of a VSC station on the local voltage profile. The selection of a suitable RPC mode can avoid undesirable control interactions (or voltage hunting issues) as mentioned in [14]. Examples of such controllers interactions have been already reported for transmission networks [15] or distribution networks [16], for other types of renewable energy systems based on VSC technology. These studies have found that in some circumstances, the $\mathrm{PF}_{\mathrm{Ctrl}}$ of a VSC unit, might induce higher operation cycles in the on-load tap changers units, when its compared against other RPC modes of a VSC unit. Nevertheless, an in-depth analysis of the influence of the RPC modes on the local voltage profiles is needed to assess the effectiveness of each RPC mode under different AC network conditions. Recently, a fundamental VS analysis has been carried out in [17] by applying a methodology based on the power flow Jacobian (like in [6, 7]) for calculating an AC voltage sensitivity factor. This methodology revealed that the steady-state voltage support provided by a basic Q_{Ctrl} could be enhanced (especially in weak network conditions), if the VSC unit's reactive power reference is modified according to a proportional AC voltage error. However, significant research effort is still needed to assess the boundaries (e.g. defined by the network strength and the reactive power capabilities of the VSC units) for the quasi-stationary voltage support provided by each RPC mode of a single-infeed VSC unit.

In this connection, and based in a reduced size power system model, this paper presents a directional derivative-based method (DDBM) which is used to evaluate and compare the conditions in which a selected RPC mode (e.g. $\mathrm{PF}_{\mathrm{Ctrl}}$, Q_{Ctrl}) of a single-infeed VSC unit can provide a superior performance in terms of quasi-stationary voltage support. Firstly, the voltage at the point of common coupling (V_{PCC}) is expressed as a mathematical function that is obtained from the power transfer equations of the reduced

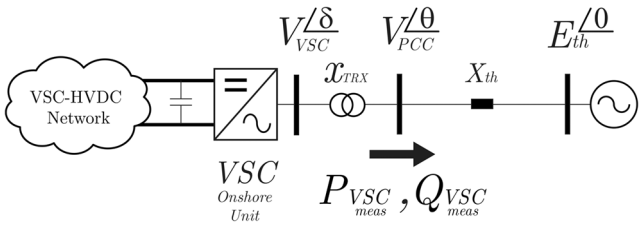

Fig. 1 *Single-infeed VSC-HVDC system model*

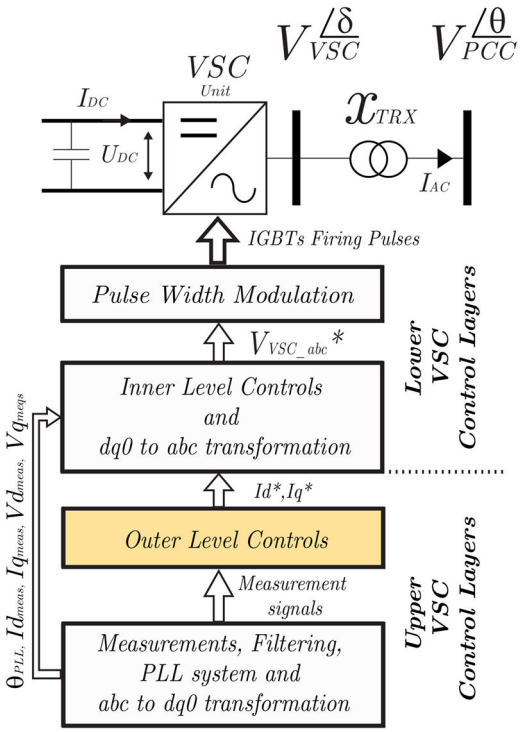

Fig. 2 *General VSC-HVDC controls layers from [14]*

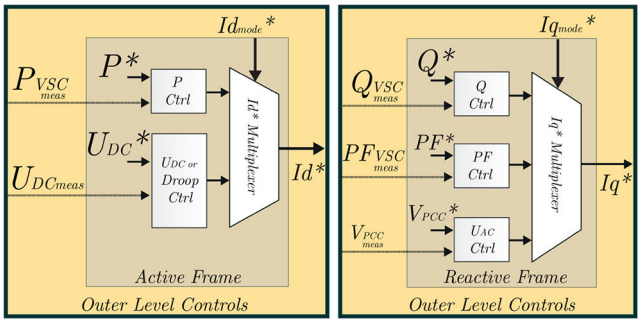

Fig. 3 *Outer level controls, general description*

size power system model considered. Secondly, the power ramp rates (**PRR**) vector of a single-infeed VSC unit is defined, based on time-varying functions describing the active power gradient (**APG**) and the reactive power gradient (**RPG**). Thirdly, the gradient vector field of the voltage at the point of common coupling (i.e. $\nabla \boldsymbol{V}_{\mathrm{PCC}}$) is described as a vector which reflects AC network strength characteristics of the reduced power system. Fourthly, the directional derivative is introduced as the scalar product between its $\nabla \boldsymbol{V}_{\mathrm{PCC}}$ and the **PRR** vectors. In this way, the directional derivative defines a time-varying sensitivity of the magnitude of V_{PCC}, in which the control actions (represented by the **PRR** vector) and the strength associated with the AC network (represented by the $\nabla \boldsymbol{V}_{\mathrm{PCC}}$) can be treated separately. Thus, the directional derivative is used to evaluate the possible trajectories determined by the **APG** and the **RPG** of the VSC unit for ensuring that a given voltage set-point is kept constant. The evaluation of these trajectories will allow generating a graphical representation for representing the level of quasi-stationary voltage support provided by the Q_{Ctrl} and the $\mathrm{PF}_{\mathrm{Ctrl}}$ modes depending on the impedance network conditions. Numerical results derived from a study case of a point-to-point (PtP)-VSC-HVDC link and its expansion to a multi-terminal (MT)-VSC-HVDC system, are executed to demonstrate the effectiveness of the proposed analytical method. This VSC-HVDC expansion has been already envisaged in a preliminary study by the authors reported in [18], and the feasibility of creating a bifurcation in the DC link has also been reported as a realistically achievable option in [19]. The remainder of the paper is organised as follows: Section 2 presents and describes the power system to be considered for the DDBM formulation and VSC's control modes commonly used by a VSC unit. Section 3 presents the power transfer and the mathematical formulation for the regulation targets of the RPC modes. Section 4 presents the bases of the DDBM for obtaining the power-trajectories presented in Section 5. Also, in Section 5, it is proposed a methodology for determining the best candidate for quasi-stationary voltage support (under low or high impedance networks conditions), based on an Euclidean distance criteria applied to the power-trajectories obtained. In Section 6, it is described as the test system to be used for verifying the findings achieved in Sections 4 and 5. The results for the point-to-point and multi-terminal operation of the test system described in Section 6 are shown in Section 7. Finally, conclusions are elaborated after Section 7.

2 System modelling

2.1 System configuration

In this work, the analysis of the quasi-stationary voltage support provided by a VSC-HVDC link to the power system is developed by considering the network representation presented in Fig. 1.

In Fig. 1, the power system is represented by an AC voltage source and a pure inductive transmission line (X_{th}), which connects the buses E_{th} and V_{PCC}, respectively. The connection of the VSC-HVDC network to the power system is achieved through the VSC unit and the transformer X_{TRX}. This VSC-HVDC network constitutes a generalisation which can represent either a meshed HVDC grid (multi-terminal VSC system) or a simple HVDC grid (point-to-point VSC system). Please also notice that the VSC unit regulates the active power P_{VSC} and reactive power Q_{VSC} at the point of common coupling or V_{PCC} bus. Additionally, it is assumed that the VSC unit is based on modular multi-level technology, which means that a filter representation (for harmonic compensation) is not required, as mentioned in [20].

2.2 VSC modelling

The modelling of a VSC-HVDC system is characterised by several control layers that have specialised functions to guarantee the energy conversion process between the DC and AC networks in which they are connected. A general description of these control layers is shown in Fig. 2.

In short, the energy conversion process in the VSC unit is developed by measuring and filtering the currents and voltages at the AC and DC sides of the VSC unit, i.e. I_{AC}, V_{PCC}, I_{DC} and U_{DC}. After a linear (*abc* to *dq*0) transformation is applied to the AC variables, to obtain the direct ($I_{d_{\mathrm{meas}}}$, $V_{d_{\mathrm{meas}}}$) and quadrature ($I_{q_{\mathrm{meas}}}$, $V_{q_{\mathrm{meas}}}$) currents and voltages, to simplify the power control of the VSC unit as detailed in [14]. As stated in [21], for a quasi-stationary (mid-term) time-scale analysis, the influence of the lower VSC control layers can be neglected. This statement allows concentrating the analysis of the quasi-stationary voltage support of the VSC unit to the outer level controls layer presented in Fig. 2, and described in Fig. 3.

As shown in Fig. 3, the outer level controls encompass two main control frames, the active frame and the reactive frame. These frames contain the control systems which generate the currents references (I_{d^*} and I_{q^*}) for the actual regulation targets in which the VSC unit has been set up. In terms of the reactive frame, any of the regulation targets Q_{Ctrl}, $\mathrm{PF}_{\mathrm{Ctrl}}$ or U_{ACCtrl} (RPC modes) can be

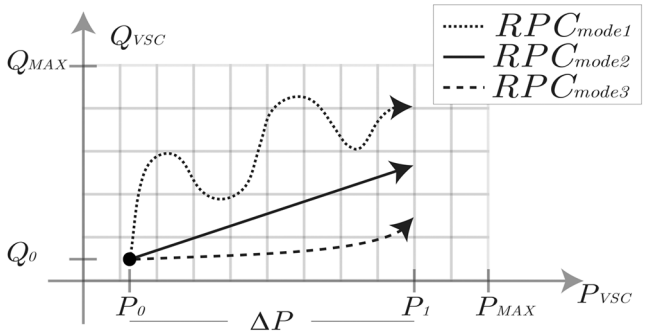

Fig. 4 *Examples of the trajectory generated by the RPC modes over a section of the VSC unit's PQ capability diagram. The evolution of the trajectories is created following a ΔP change from the P_o, Q_o steady-state power conditions*

selected by the VSC unit operator through the $I^*_{q\text{mode}}$ signal (Fig. 3). Similarly, any of the regulation targets of the active frame can be selected through the $I^*_{d\text{mode}}$ signal. Please note that, the VSC unit regulation targets selection P_{Ctrl}, U_{DCCtrl} or $\text{Droop}_{\text{Ctrl}}$ must be aligned with the VSC-HVDC network configuration (point-to-point or multi-terminal VSC system).

3 Analytical formulation for quasi-stationary AC voltage support of a VSC unit

3.1 Steady-state power and voltage equations

The mathematical descriptions of the RPCs and the power system are formulated here, to highlight the interplay between the regulation RPC's modes with the quasi-stationary voltage analysis. First of all, the steady-state equations for the power system shown in Fig. 1 are presented in the following equations:

$$P_{\text{VSC}} = \frac{|V_{\text{PCC}} \parallel E_{\text{th}}|\sin(\theta)}{X_{\text{th}}} \tag{1}$$

$$Q_{\text{VSC}} = \frac{|V_{\text{PCC}}|^2}{X_{\text{th}}} - \frac{|V_{\text{PCC}} \parallel E_{\text{th}}|\cos(\theta)}{X_{\text{th}}} \tag{2}$$

If the power system variables X_{th} and E_{th} are assumed to be constant, then it is possible to describe the V_{PCC} voltage in terms of P_{VSC} and Q_{VSC} as shown in (3). It is clear then that the V_{PCC} profile will be influenced by the control schemes used to modulate the active and reactive power produced by the VSC unit. However, these power modulations can be appreciated as the corresponding paths generated by the control modes within the PQ capability diagram (limits) of the VSC unit, as shown in Fig. 4.

$$V_{\text{PCC}}(P_{\text{VSC}}, Q_{\text{VSC}}) = \sqrt{\frac{|E_{\text{th}}|^2}{2} + X_{\text{th}}Q_{\text{VSC}} + \sqrt{\frac{|E_{\text{th}}|^4}{4} + |E_{\text{th}}|^2 X_{\text{th}}Q_{\text{VSC}} - X_{\text{th}}^2 P_{\text{VSC}}^2}} \tag{3}$$

Thus, the study of the quasi-stationary AC voltage's profile support by means of a VSC unit can be tackled as a power-trajectories analysis problem. The development of this analysis will start by proposing in Section 3.2, a mathematical formulation for the regulation targets of each RPC mode, which will be posteriorly used by the DDBM in Section 4.

3.2 Mathematical formulations for the VSC's RPC modes operation

The mathematical formulation for each RPC mode can be defined to express their regulation targets as presented in the following equations:

$$Q_{\text{Ctrl}} \Rightarrow \frac{Q^* - Q_{\text{meas}}}{\Delta t} = \frac{\Delta Q_{\text{VSC}}(t)}{\Delta t} = 0 \tag{4}$$

$$\text{PF}_{\text{Ctrl}} \Rightarrow \frac{\text{PF}^* - \text{PF}_{\text{meas}}}{\Delta t} = \frac{\Delta \text{PF}_{\text{VSC}}(t)}{\Delta t} = 0 \tag{5}$$

$$U_{\text{ACCtrl}} \Rightarrow \frac{V^*_{\text{PCC}} - V_{\text{PCC}_{\text{meas}}}}{\Delta t} = \frac{\Delta V_{\text{PCC}}(t)}{\Delta t} = 0 \tag{6}$$

In this paper, it is assumed that PI regulators are used in each RPC mode. If other types of regulators (e.g. only proportional controllers) are considered, the mathematical formulations in (4)–(6) do not hold and the analysis of power-trajectories should be performed by executing time-domain simulations which can be very computationally expensive. Therefore, by considering PI regulators, it is assumed that they can ensure that for any $\Delta t > 0$, in (4)–(6), each mathematical relationship can be satisfied. In this way, several implications of the use of each RPC mode can be analysed. First, if the Q_{Ctrl} is chosen, the V_{PCC} profile deviation will depend exclusively on the active power changes as shown in (3). Second, if the PF_{Ctrl} is chosen, the magnitudes of the **APG** and the **RPG** of the VSC unit will be related, as shown in (7). Thus the PF_{Ctrl} will generate a dependence between the Q_{VSC} and the P_{VSC} variables presented in (3) by means of a proportional constant, the λ factor. This factor represents the steady-state power ratio $|Q_{\text{oVSC}}/P_{\text{oVSC}}|$ to be maintained by the PF_{Ctrl}.

$$\text{RPG} = \lambda * \text{APG} \tag{7}$$

The third deduction is referred to as the U_{ACCtrl} mode analysis. The mathematical relationship presented in (6) can be perceived as the rate of change of the V_{PCC} w.r.t. time. Consequently, the analysis V_{PCC} profile defined by (6) can be tackled by means of the description of two main elements: the partial derivatives of (3) and the description of the rate of changes of P_{VSC} and Q_{VSC}, respectively. This analysis will allow illustrating the power-trajectory description for each RPC mode (4)–(6) using the DDBM presented in Section 4.

4 DDBM for VSC unit power-trajectory description

4.1 Definition and interpretation of dynamic vectors

The deployment of the DDBM for quasi-stationary voltage support analysis of a single infeed VSC unit will start by defining the vector spaces represented by the two diagrams shown in Fig. 5. In this work, the first diagram (presented in Fig. 5*a*) represents the vector space that contains the directional vector **PRR** (or the power ramp-rate vector of the VSC unit). As seen in Fig. 5*a*, the directional **PRR** vector is comprised by the **APG** magnitude (i.e. $(\text{d}P_{\text{VSC}}(t)/\text{d}t)$ value), and the **RPG** magnitude (i.e. $(\text{d}Q_{\text{VSC}}(t)/\text{d}t)$ value). As the control modes of the VSC unit regulate the P_{VSC} and the Q_{VSC} provided to the power system, the rate of changes of the P_{VSC} and Q_{VSC} (i.e. **APG** and **RPG**) are also defined by the control modes used by the VSC unit.

Ergo, the directional **PRR** vector (in Fig. 5*a*) and its corresponding trajectory (in Fig. 5*c*) are *shaped* by the control systems used by the VSC unit. For instance, during steady-state time periods, the norm of the **PRR** vector is null since its **APG** and the **RPG** components (in Figs. 5*a* and *c*) have zero magnitudes during these time frames. The second diagram (presented in Fig. 5*b*) represents the vector space in which the gradient vector field of the V_{PCC} function (shown in (3)), is an exhibit, that is to say, $\nabla \boldsymbol{V}_{\text{PCC}}$ vector. As shown in Figs. 5*b* and *d*, the $\nabla \boldsymbol{V}_{\text{PCC}}$ vector is comprised of the partial derivatives $\partial V_{\text{PCC}}/\partial P_{\text{VSC}}$ and $\partial V_{\text{PCC}}/\partial Q_{\text{VSC}}$, which are mainly defined by the power systems parameters, X_{th} and E_{th} expressed in (3). Consequently, the *shape* of the trajectory exhibited by the $\nabla \boldsymbol{V}_{\text{PCC}}$ vector (in Fig. 5*d*) is fundamentally determined by these power system parameters.

As the trajectories shown by the $\nabla \boldsymbol{V}_{\text{PCC}}$ vector (in Fig. 5*d*) and the **PRR** vector (in Fig. 5*c*) evolve in a time frame axis, $\nabla \boldsymbol{V}_{\text{PCC}}$ and **PRR** represent indeed dynamic vectors. These dynamic vectors

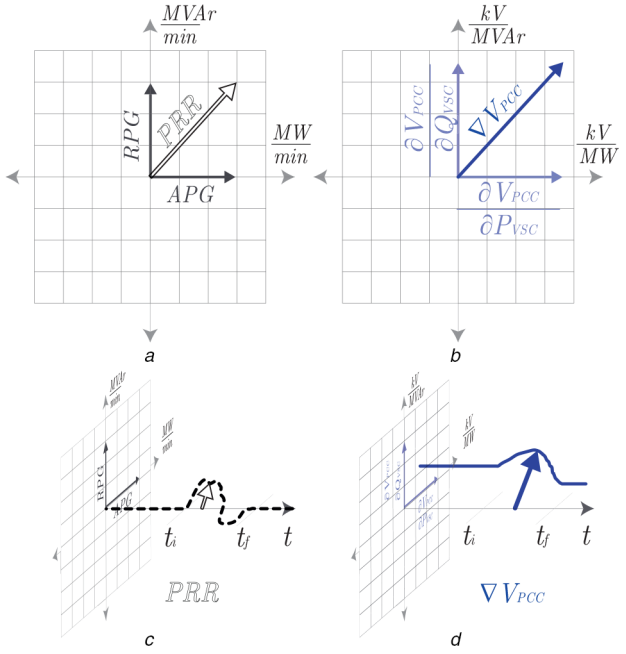

Fig. 5 *Space-time representations of the dynamic vectors **PRR** and $\nabla \boldsymbol{V}_{PCC}$ **(a)** VSC power ramp-rate diagram, **(b)** **PCC**-Voltage's gradient diagram, **(c)** Space-time diagram of **PRR**, **(d)** Space-time diagram of $\nabla \boldsymbol{V}_{PCC}$*

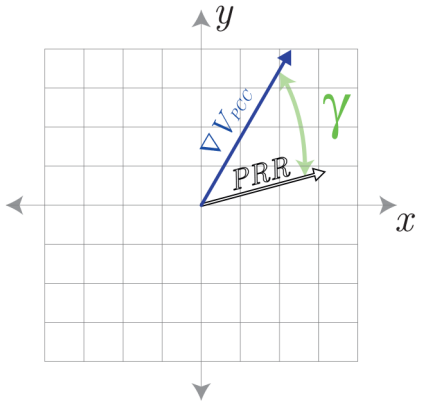

Fig. 6 *The γ angle (in green) representing the angular difference between the $\nabla \boldsymbol{V}_{PCC}$ and **PRR** dynamic vectors shown in Fig. 5c and Fig 5d*

perspective allows to expose in a graphical and individual manner, the two main characteristics for the quasi-stationary V_{PCC} support. On the one hand, the power system features such as the X_{th} and the E_{th} (exhibited by the $\nabla \boldsymbol{V}_{PCC}$ trajectory) and, on the other hand, the power modulation executed by the control modes used by the VSC unit (exhibited by the **PRR** trajectory).

The interaction analysis of the dynamic vectors trajectories will lead to the formulation of an instantaneous voltage sensitivity factor (IVSF) as presented in the following equation:

$$\text{IVSF} = \nabla \boldsymbol{V}_{PCC} \cdot \mathbf{PRR} \tag{8}$$

The IVSF is defined as the scalar product between the dynamic vectors $\nabla \boldsymbol{V}_{PCC}$ and **PRR**. This scalar product defines the interaction between **PRR** (VSC's control modes) with $\nabla \boldsymbol{V}_{PCC}$ (AC network strength) and constitutes the formulation of the directional derivative method as a way to describe the rate of change of V_{PCC} in Fig. 1. If **PRR** and $\nabla \boldsymbol{V}_{PCC}$ are projected over the same Cartesian coordinate system (as shown in Fig. 6), the angle γ between them can be defined as presented in the following equation:

$$\gamma = \text{atan}\left(\frac{\partial V_{PCC}/\partial Q_{VSC}}{\partial V_{PCC}/\partial P_{VSC}}\right) - \text{atan}\left(\frac{\text{RPG}}{\text{APG}}\right) \tag{9}$$

The mathematical formulations (8) and (9) depend on two main factors: the explicit knowledge of the vector field of V_{PCC} (i.e. $\nabla \boldsymbol{V}_{PCC}$), and the **APG** and **RPG** modulations executed by each control mode. The explicit knowledge of the vector field of the V_{PCC} is known since, the function of V_{PCC} has been explicitly defined in (3). Now, the **PRR** formulation can be elaborated based on the RPC mode formulations established in (4)–(7) and will be described from Section 4.2 to Section 4.5 to define the power-trajectories shown in Section 5.

4.2 U_{ACCtrl} mode analysis based on DDBM

The regulation target of the U_{ACCtrl} mode can be expressed in terms of the DDBM, by imposing to the IVSF, the mathematical restriction stated in (6). This can be done by obtaining the partial derivatives of (3) and by defining the magnitude of the **RPG** (illustrated in Fig. 5*a*) as expressed in the following equation:

$$\text{RPG} = -\text{APG} * \frac{\partial V_{PCC}/\partial P_{VSC}}{\partial V_{PCC}/\partial Q_{VSC}} \tag{10}$$

When (10) is substituted in (9), the γ angle (in Fig. 6) becomes $\pm(\pi/2)$. This means that, from the DDBM point of view, the role of the U_{ACCtrl} mode is to modulate the **RPG** magnitude such that, the **PRR**'s trajectory be orthogonal to the $\nabla \boldsymbol{V}_{PCC}$'s trajectory while a change in P_{VSC} is executed.

4.3 PF_{Ctrl} mode analysis based on DDBM

The regulation target of the PF_{Ctrl} mode can be expressed in terms of the DDBM, by evaluating the condition presented in (7) into the DDBM formulation shown in (9). If the partial derivative $\partial V_{PCC}/\partial P_{VSC}$ (which is a function of X_{th} as mentioned in Section 4.1) is assumed to be very low (which is a valid assumption for low impedance networks), the γ angle can be expressed as presented in the following equations:

$$\gamma_{PF_{Ctrl}} \simeq \pm\frac{\pi}{2} - \text{atan}(\lambda) \tag{11}$$

Now, if the magnitude of the IVSF in (8) is computed by considering the linear relationship presented in (7), the voltage deviation experienced by V_{PCC} (as a consequence of having the VSC unit in Fig. 1, operating in PF_{Ctrl} mode) will be defined by the following equation:

$$\left|\text{IVSF}_{PF}\right| = \left|\nabla V_{PCC} \parallel \text{APG}\right|\sqrt{1+\lambda^2}\left|\cos(\gamma_{PF_{Ctrl}})\right| \tag{12}$$

It can be seen from (12) that the magnitude of the IVSF gets amplified depending on the steady-state power ratio, λ value. Therefore, it is (in general) advisable to decrease the λ ratio for the operation of the PF_{Ctrl} mode by setting up in the PF_{Ctrl}, a PF reference value (PF^*) close to the unity.

4.4 Q_{Ctrl} mode analysis based on DDBM

Similar to the previous two RPC modes analysis, the regulation target of the Q_{Ctrl} mode will start by integrating the mathematical condition presented in (4) into the DDBM formulation shown in (8) and (9). If again, the partial derivative $\partial V_{PCC}/\partial P_{VSC}$ is assumed to be very low, then, the associated IVSF's magnitude and γ angle (for the Q_{Ctrl} mode DDBM analysis) can be described by the following equations:

$$\gamma_{Q_{Ctrl}} \simeq \pm\frac{\pi}{2} \tag{13}$$

$$\left|\text{IVSF}_{Q}\right| = \left|\nabla V_{PCC} \parallel \text{APG} \parallel \cos(\gamma_{Q_{Ctrl}})\right| \tag{14}$$

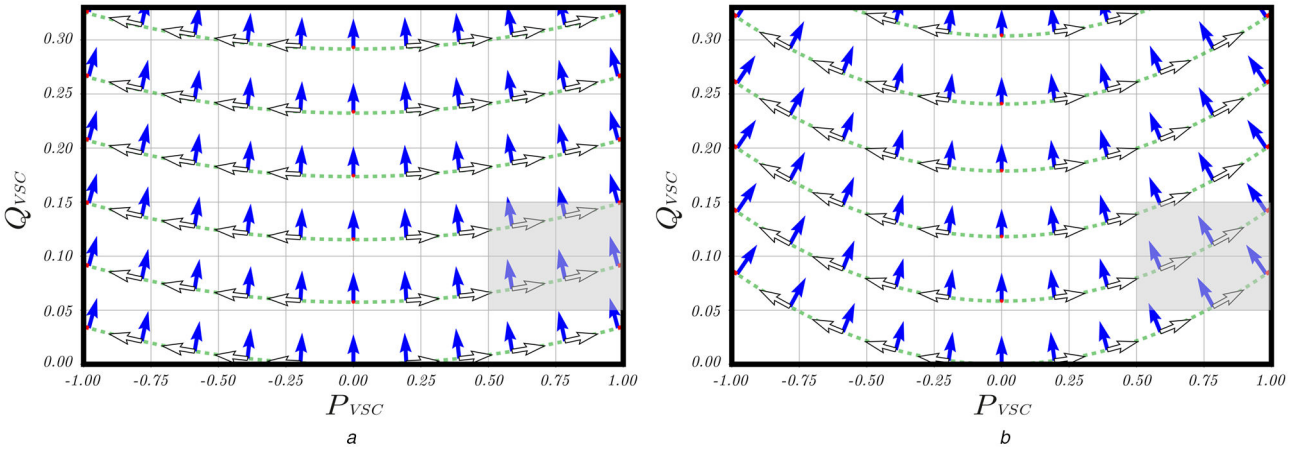

Fig. 7 *The orthogonality condition between **PRR** and $\nabla \boldsymbol{V}_{\mathrm{PCC}}$ creating the power-trajectories of the U_{ACCtrl} (dotted-green lines) for different the X_{th} conditions presented in Table 1.*

(a) The vectors fields of **PRR** and $\nabla \boldsymbol{V}_{\mathrm{PCC}}$ projected over the PQ capability diagram of a VSC unit connected to a low impedance network ($\mathrm{X_{thlow}}$), ***(b)*** The vectors fields of **PRR** and $\nabla \boldsymbol{V}_{\mathrm{PCC}}$ projected over the PQ capability diagram of a VSC unit connected to a high impedance network ($\mathrm{X_{thhigh}}$)

Table 1 VSC unit and power system features for Fig. 7 and Fig. 9

S_{BASE}	E_{th} (V_{BASE})	P_{MAX}, pu	Q_{MAX}, pu	$X_{\mathrm{th_{low}}}$, pu	$X_{\mathrm{th_{high}}}$, pu
700 MVA	405 kV	1	0.3286	0.0196	0.1225

If the same steady-state power conditions P_{oVSC}, Q_{oVSC} and |APG| are considered for (12) and (14), the comparison of the IVSF's magnitudes will be determined by the constant $\sqrt{1+\lambda^2}$ and the corresponding γ angles values presented in (11) and (13). In general, these two equations would lead to conclude that the $\mathrm{PF_{Ctrl}}$ is always the less attractive option for voltage support if it is compared against the Q_{Ctrl}. This conclusion has been also verified by performing specific field tests in [15]. However, the influence of $\partial V_{\mathrm{PCC}}/\partial P_{\mathrm{VSC}}$ on the γ magnitude, has not been so far considered for analysing the quasi-stationary voltage support provided by a single-infeed VSC unit. In other words, (11) and (13) have been obtained based on the assumption of having a very low value for the partial derivative $\partial V_{\mathrm{PCC}}/\partial P_{\mathrm{VSC}}$. Hence, if this assumption is not considered anymore (i.e. power system having high impedance network conditions), the magnitude of the γ angles will be entirely determined by the evolution of the $\nabla \boldsymbol{V}_{\mathrm{PCC}}$ vector components (Fig. 5*b*). Thus, depending on the steady-state power conditions (P_{oVSC} and Q_{oVSC}) and, the X_{th} value, the $\mathrm{PF_{Ctrl}}$ mode might provide a better voltage support if it is compared to the voltage support provided by the Q_{Ctrl} mode. This statement will be thoroughly analysed in Section 5.

4.5 Influence of the VSC-HVDC network configuration on the **APG** *vector magnitude formulation*

The analysis of the active frame control modes, in terms of the DDBM, can be tackled by describing the implications of each regulation target (P_{Ctrl}, U_{DCCtrl}, or $\mathrm{Droop_{Ctrl}}$) over the **APG** magnitude. Typically, the **APG** value is a constant parameter specified by the owner of the PtP-VSC-HVDC system. Hence, if the active power balance is ensured within the HVDC network, the active power changes in one VSC unit (operating in P_{Ctrl}) will be reflected in the other VSC unit (operating in U_{DCCtrl}). Thus, the **APG** magnitude in a PtP-VSC-HVDC system operation will be equivalent for both VSC units as described in the following equation:

$$\mathrm{PtP_{Op}} \Rightarrow \left|\mathrm{APG_{U_{DCCtrl}}}\right| = \left|\mathrm{APG_{P_{Ctrl}}}\right| \tag{15}$$

On the other hand, in an MT-VSC-HVDC system, the active power balance regulation usually involves additional control strategies like the $\mathrm{Droop_{Ctrl}}$ mode. This strategy allows disseminating the regulation of the DC voltage within the MT-VSC-HVDC network, by distributing the DC power flow between the VSC units accordingly to a proportional constant, the K_{Droop}.

Since the MT-VSC-HVDC systems are prone to include renewable energy sources (RESs), the resulting **APG** values of the VSC units belonging to the MT-VSC-HVDC network, might not be constant. Therefore, a proportional factor (η) is defined to simultaneously consider the effects of the DC power flow strategies utilised by all VSC units within an HVDC network. Concretely, the factor η will allow to express the **APG** value for each VSC unit within the MT-VSC-HVDC network as defined in the following equation:

$$\mathrm{MT_{Op}} \Rightarrow \left|\mathrm{APG_{VSC_i}}\right| = \eta_i \left|\mathrm{APG_{RES}}\right| \tag{16}$$

As seen in (16), the **APG** value of a particular VSC unit i (e.g. $\mathrm{APG_{VSC_i}}$), depends on the active power gradient associated to the RES (e.g. $\mathrm{APG_{RES}}$) included within the VSC-HVDC network. The range of η_i in (16) goes from a non-influence of the $\mathrm{APG_{RES}}$ (e.g. $\eta_i = 0$) to a maximum influence of the $\mathrm{APG_{RES}}$ (e.g. $\eta_i = 1$). The utilisation of the η_i factor will be exemplified by considering a three-terminal (MT-VSC-HVDC) system described in Section 6.

5 Graphical description of the DDBM for RPC's power-trajectories analysis

The mathematical formulations described in Section 4 have geometrical implications that will be elaborated in this section. The orthogonality condition mentioned in Section 4.1 for the **PRR** dynamic vector, can be illustrated by determining the V_{PCC}'s vector field and project it over the PQ capability diagrams, as shown in Figs. 7*a* and *b*. The vector field of V_{PCC} can be computed from (3) if the power system features (X_{th} and E_{th} in Fig. 1) and the VSC unit power limits (P_{MAX}, Q_{MAX}) are known. In this work, the VSC power limits and power system features are presented in Table 1 and were obtained from [3, 12], respectively.

Once the $\boldsymbol{V}_{\mathrm{PCC}}$'s vector field is known (i.e. $\nabla \boldsymbol{V}_{\mathrm{PCC}}$), the VSC-HVDC network configuration needs to be determined. For a PtP-VSC-HVDC system, the **APG** magnitude is assumed to be constant as discussed in Section 4.4. Consequently, the orthogonality condition produced by the U_{ACCtrl} mode (10), will generate the **PRR**'s vector fields as the ones presented in Figs. 7*a* and *b*. The dash lines shown in Figs. 7*a* and *b* represent the power trajectories in which the regulation target of the U_{ACCtrl} mode is achieved (6). In other words (and from the DDBM point of view), the power-trajectories in which the scalar product of the $\nabla \boldsymbol{V}_{\mathrm{PCC}}$ and the **PRR** is null. Moreover, these dash lines, exhibit different curvature ratios, which are a consequence of the difference

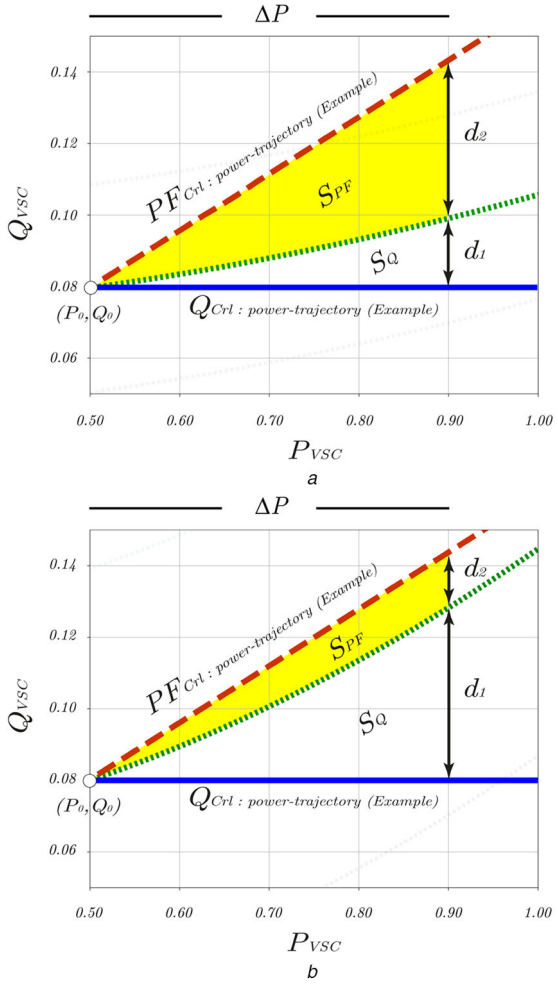

Fig. 8 *Geometrical comparison of the power-trajectories for each RPC mode for the same DP and (P_o, Q_o) steady-state power conditions.*
(a) S_Q area describing the Q_{Ctrl} mode as the second-best option for quasi-stationary voltage support, ***(b)*** S_{PF} area describing the PF_{Ctrl} mode as the second-best option for quasi-stationary voltage support

between the X_{th} network conditions in Table 1. Thus, it can be seen that the evolution of the **RPG** magnitude (i.e. the rate of change of reactive power in Fig. 5*a*) for a high impedance network (Fig. 7*b*), is prone to be higher than the one observed for the low impedance network (Fig. 7*a*) case. Therefore, the quasi-stationary voltage support of a VSC unit, for a high impedance network, is conditioned by its capability of providing fast reactive power modulation while an active power changes occur. This condition might constitute a challenge in terms of the VSC unit design and the VSC unit's coordination with other voltage support systems (e.g. the transformer tap changers) [16].

Conversely, in Fig. 7*a*, the associated **PRR** vector field is not prone to evolve (increase their **RPG** magnitude, cf. Fig. 5*a*) as fast as the **PRR** vector field, presented for the high impedance network case (i.e. Fig. 7*b*). Hence, the Q_{Ctrl} mode might be considered as *a good option* for providing quasi-stationary voltage support in V_{PCC} during low impedance network conditions. However, in order to illustrate the meaning of *a good option* for the quasi-stationary voltage support (in either high or low impedance networks), a comparative assessment, based on a Euclidean-distance criterion, is proposed.

The Euclidean-distance criteria will depend on the explicit knowledge of the points belonging to the power-trajectories generated by each RPC mode. Thus, the determination of these points is a necessary step for the comparison process between the different quasi-stationary voltage support strategies of a VSC unit. The power-trajectories generated by the U_{ACCtrl} mode (shown as dash lines in Figs. 7*a* and *b*) can be obtained by computing the level set curves from (3). On the other hand, the power-trajectories generated by the Q_{Ctrl} and the PF_{Ctrl} modes are based on the operational ranges specified by the VSC unit operator and will be illustrated by using Figs. 8*a* and *b*. Please note that Figs. 8*a* and *b* constitute zooming of the highlighted grey sections, presented in the *PQ* capability diagram of Figs. 7*a* and *b*, respectively.

The formulations presented in (4) and (7), automatically define the behaviour of the **RPG** magnitude (Fig. 5*a*) for the Q_{Ctrl} and the PF_{Ctrl} modes, for any technically feasible **APG** value (or VSC-HVDC network configuration, cf. Section 4.4). These formulations would indicate that the points which belong to the power-trajectories generated by either the Q_{Ctrl} or the PF_{Ctrl} mode, can be represented by means of a straight line or a sloped line as shown in Figs. 8*a* and *b*. Consequently, the Euclidean-distances between the points belonging to each power-trajectory can be used, to define the *S* factors (Riemann's sums) presented in the following equation:

$$S_Q = \sum_{i=0}^{n} |d_1(P_i) \parallel \Delta P_i|$$
$$S_{PF} = \sum_{i=0}^{n} |d_2(P_i) \parallel \Delta P_i| \quad (17)$$

As it can be seen in Figs. 8*a* and *b*, the d_1 and d_2 values represent the distances between the power-trajectories produced by the Q_{Ctrl} and the PF_{Ctrl} modes w.r.t. the U_{ACCtrl} power-trajectory, respectively. Please note that the distance values depend on the active power level provided by the VSC unit, and the impedance network condition X_{th}. In (17), the S_Q and S_{PF} factors (respectively, the white and yellow areas in Fig. 8) represent the equivalent areas generated when an active power change (ΔP) occurs in the VSC unit, from its initial steady-state power conditions P_{oVSC} and Q_{oVSC}, (i.e. (P_o, Q_o) in Fig. 8). Then, if the S_Q and the S_{PF} factors values are compared, the one that possesses the minimum value (minimum area) will be closest to the U_{ACCtrl} power-trajectory. In other words, the minimum *S* factor identifies the RPC control mode, which produces the smallest quasi-stationary voltage deviation during an active power change in the VSC unit. From Fig. 8*a*, it can be noticed that for the $X_{th_{low}}$ case, the area represented by the S_Q factor is smaller than the area represented by the S_{PF} factor. This means that the Q_{Ctrl} mode can be considered as *a good option* for the quasi-stationary voltage support of V_{PCC} if it is compared against the PF_{Ctrl} mode for the same initial steady-state power conditions P_o, Q_o. However, in Fig. 8*b*, the curvature ratio associated to the U_{ACCtrl} power-trajectory is shorter, which means that the distance d_2 will also be shorter if it is compared against the one presented in Fig. 8*a*. Thus, for this particular example, the area represented by the S_{PF} factor is smaller than the one represented by the S_Q factor. Consequently, the PF_{Ctrl} mode can be considered as *a good option* for quasi-stationary voltage support of V_{PCC} if it is compared against the Q_{Ctrl} mode for the same initial P_o, Q_o steady-state power conditions. Thus, the explicit determination of the power-trajectories, the selection of the steady-state power condition (P_o, Q_o) and the descriptions of the $\nabla \boldsymbol{V}_{PCC}$ and the **PRR** dynamic vectors represent the bases for the quasi-stationary voltage support analysis (of a single-infeed VSC unit), provided by DDBM.

The graphical methodology based on the *S* factors constitutes the first step to quickly provide a comparative assessment between the Q_{Ctrl} and the PF_{Ctrl} modes w.r.t. an ideal U_{ACCtrl} mode. However, some questions might appear, especially when the values of the S_{PF} and S_Q are quite similar. For these cases, it is necessary to introduce a second (more precise) comparative criteria in which the values of each $d_1(P_i)$ and $d_2(P_i)$ (belonging to a specific power-trajectories analysis) are contrasted. This more precise comparative criterion basically provides two main features. First, it allows to substantially increase the degree of accuracy for comparing the level of quasi-stationary voltage support for each RPC mode (e.g. Q_{Ctrl} and PF_{Ctrl}). Second, it allows determining the steady-state power conditions (e.g. P_o, Q_o), in which the Q_{Ctrl} mode or the PF_{Ctrl}

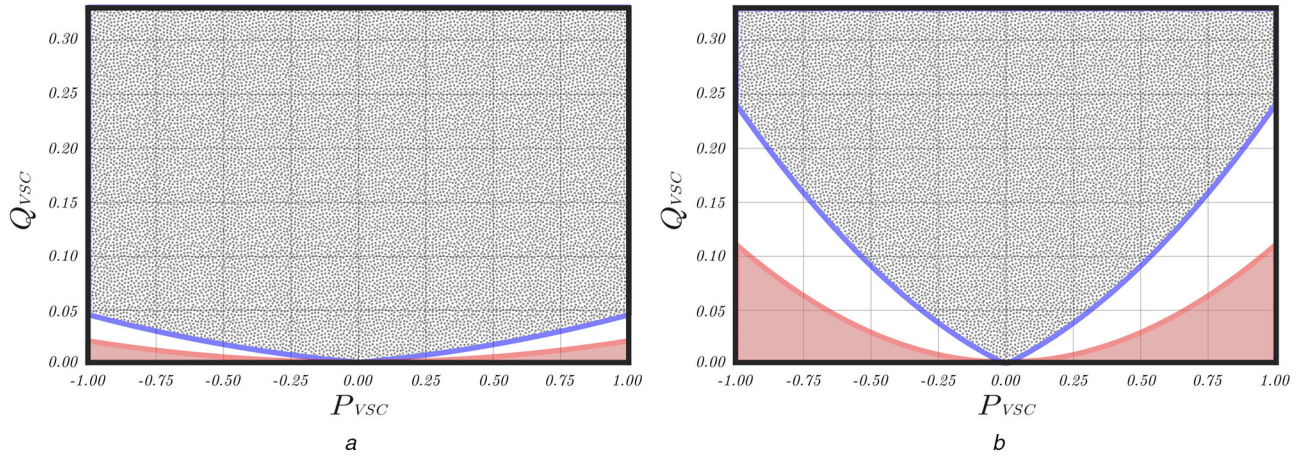

Fig. 9 *PQ capability diagram of a VSC unit showing the areas in which the Q_{Ctrl} and PF_{Ctrl} represent the second-best option for quasi-stationary voltage support under different AC network conditions*

(a) Exhibiting the Q_{Ctrl} mode (dotted grey area) as the second-best choice under a low impedance network condition ($X_{th_{low}}$), ***(b)*** Exhibiting the reduction of the Q_{Ctrl} mode (dotted grey area) and the increment of the PF_{Ctrl} mode (solid red area) under a high impedance network condition ($X_{th_{high}}$)

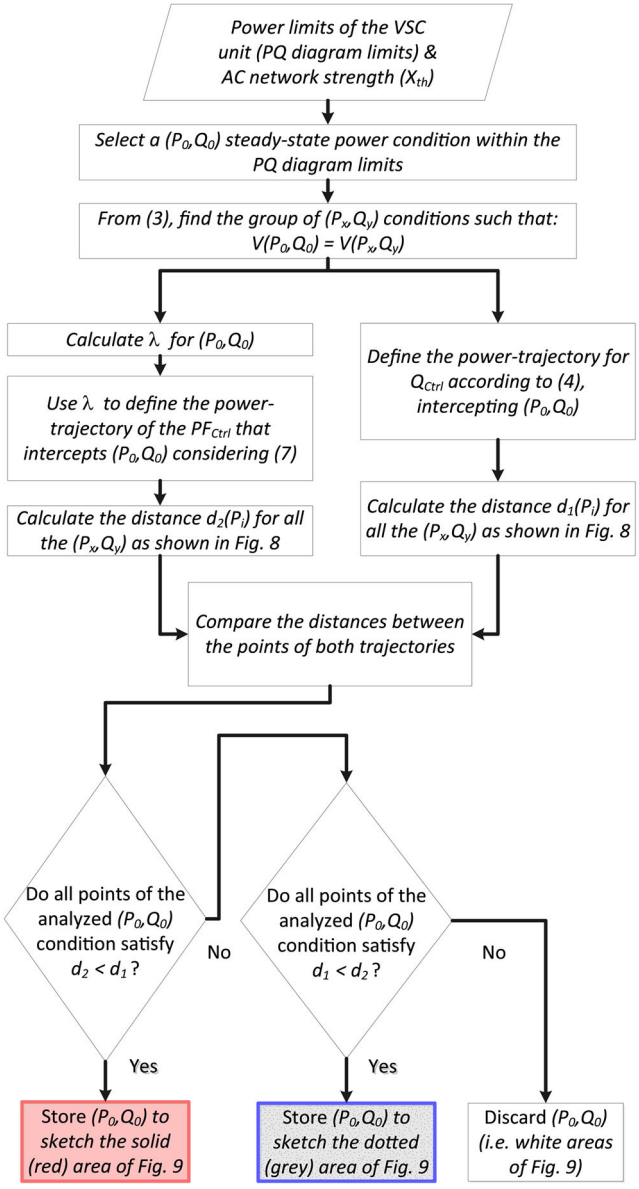

Fig. 10 *Flowchart of the MATLAB code showing the analytical process for determining if one steady-state power condition (P_o, Q_o) can be considered to generate the (red) solid, the (grey) dotted or the white area*

mode presents a superior performance (one respect to the other) for quasi-stationary voltage support.

The implementation of the second comparative criteria was developed as a MATLAB code in which all the possible steady-state points and power-trajectories for the three RPC modes of the VSC unit were considered. Finally, the execution of the MATLAB code produced the areas presented in Figs. 9*a* and *b*, respectively. The dotted (grey) regions in Figs. 9*a* and *b* define the steady-state power conditions in which the Q_{Ctrl} will exhibit better performance in terms of quasi-stationary voltage support rather than the PF_{Ctrl} mode.

Conversely, the solid (red) regions in Figs. 9*a* and *b* define the steady-state power conditions in which the PF_{Ctrl} will exhibit better performance in terms of quasi-stationary voltage support rather than the Q_{Ctrl}. Finally, the white areas in Figs. 9*a* and *b* represent the steady-state power conditions in which the second-best option for quasi-stationary voltage support cannot be entirely attributed to a single RPC mode, that is to say, the PF_{Ctrl} or the Q_{Ctrl}. In the white areas, the level of quasi-stationary voltage support obtained will also depend on the amount of active power change (increment or decrement) experienced by the VSC unit studied. The corresponding flowchart of the MATLAB code executed is shown in Fig. 10.

It can also be noticed that the sizes of each region in Figs. 9*a* and *b* are comparatively different. This means that the evolution of the impedance network (i.e. from $X_{th_{low}}$ to $X_{th_{high}}$) will alter the conditions (i.e. Fig. 9 areas) in which an RPC mode can be considered as an attractive option for providing quasi-stationary voltage support. In that sense, the DDBM provides a way to graphically compare the performance of the Q_{Ctrl} verses PF_{Ctrl} by simultaneously considering different AC network strength levels. For instance, using the Q_{Ctrl} in Fig. 9*a* for a steady-state power condition equal to $Q_o = 0.15$ and $P_o = 0.50$ will create less V_{PCC} deviations than using PF_{Ctrl} for the same (P_o, Q_o) conditions. However, using the Q_{Ctrl} for a steady-state power condition equal to $Q_o = 0.05$ and $P_o = 0.75$ in Fig. 9*b* will generate a bigger V_{PCC} deviation if it's compared against the one generated by the PF_{Ctrl} mode. This does mean that by assuming an ideal U_{ACCtrl} mode, the DDBM provides a fast way to illustrate which RPC mode is the worst and the second most attractive option for providing quasi-stationary voltage support based on the comparison of the distances (i.e. d_1 and d_2) obtained. It is worth remembering that the graphical DDBM analysis conducted so far has been based on the constant **APG** magnitude assumption for each RPC mode. However, the variable nature of the **APG** (most likely expected for a VSC unit belonging to an MT-VSC-HVDC network) will be cover in Section 6. This analysis will be carried out by executing simulation experiments using a quasi-stationary phasor (or RMS) model for an

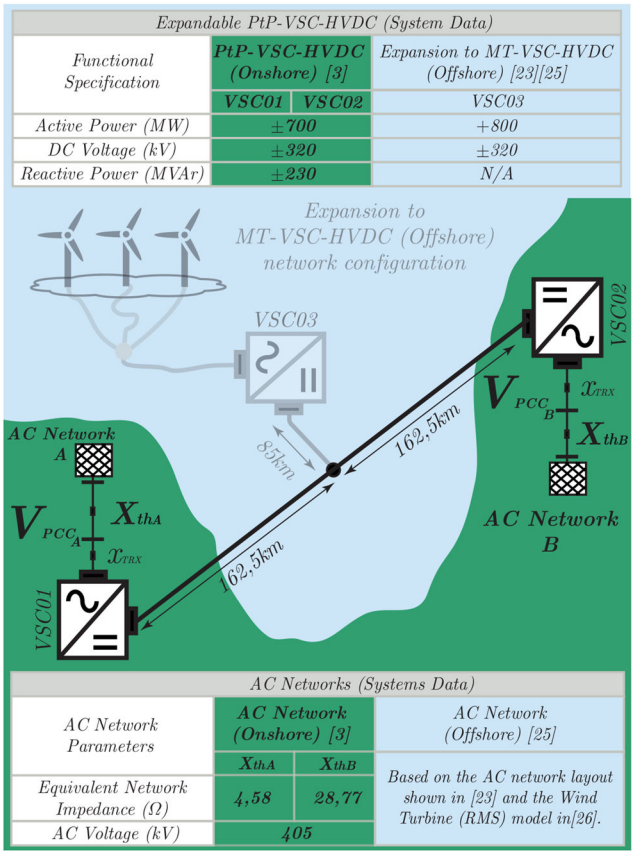

Fig. 11 *Expandable PtP-VSC-HVDC network. The PtP-VSC-HVDC network configuration represented by the elements highlighted in black colour and the MT-VSC-HVDC expansion represented by the elements highlighted in grey colour*

Table 2 Description of the Multi-terminal operation (power flow) cases for the Expandable PtP-VSC-HVDC system of Fig. 11

Multi-terminal operation	$\eta_{1\text{VSC01}}$	$\eta_{2\text{VSC02}}$	$\eta_{3\text{VSC03}}$
case 1	0.5	0.5	1
case 2	0.02	0.98	1

expandable PtP-VSC-HVDC network, which will be introduced in Section 6.

6 Overall description for the test system

6.1 Expandable PtP-VSC-HVDC network

In this work, the expandability of a PtP-VSC-HVDC network is referred to the ability of such a system to operate in MT-VSC-HVDC network configuration when one or more VSC stations are connected (added) to the existing PtP-VSC-HVDC network as shown in Fig. 11. This expandability property constitutes a challenge, in terms of the technical interoperability between several VSC units, especially if they belong to different converters manufacturers [22]. However, in terms of the DC power flow management, a solution has been already proposed in [23]. As described in [23], the expandability property of a PtP-VSC-HVDC system can be ensured if a primary control interface (PCI) for DC voltage regulation is utilised. In summary, the PCI requires the knowledge of the limits concerning the active power and the DC voltage for each VSC unit, to execute the DC power flow control. This means that the operation of an *expandable* PtP-VSC-HVDC network is bounded by the operational features (functional limits) of the VSC units belonging to the PtP-VSC-HVDC network. Therefore, the simulations experiments for analysing the quasi-stationary voltage support of a single-infeed VSC unit will be developed for an *expandable* PtP-VSC-HVDC system based on [23]. In this way, the combined effects of the RPC modes with a fixed or a variable **APG** value will be determined by simultaneously considering different AC network strength levels.

6.2 Simulation setup for the PtP and the MT-VSC-HVDC configuration

The simulation setup presented in this section has been developed utilising the software DIgSILENT PowerFactory 2018. Additionally, the simulation model used for the *expandable* PtP-VSC-HVDC network and the AC networks utilised in this work has been obtained from [3, 12, 24, 25], respectively. For the sake of illustration, it is assumed that the expansion of the PtP-VSC-HVDC network to an MT-VSC-HVDC configuration concerns with the integration of an offshore wind farm (OWF) through a third terminal (VSC03 unit), as shown in Fig. 11. It can be seen that the system data presented in Fig. 11 is linked with the information provided in Table 1. Therefore, the vector fields shown in Figs. 7*a* and *b*, represent the ones associated with the onshore VSC units, VSC01 and VSC02 (shown in Fig. 11), respectively. The islanded control scheme described in [14] has been implemented for the VSC03 unit to provide the corresponding AC voltage reference to the OWF's network. The control schemes for the OWF units have been implemented based on the modelling work presented in [26]. Additionally, the wind power generation profile associated with the OWF units was defined, based on real wind power generation data obtained from a European transmission system operator in [27].

In [23], it is described that the essential requirement that the PCI demands to execute the DC power flow management is the access to the DC voltage reference's regulation in those VSC units selected to perform such tasks in the multi-terminal VSC-HVDC network. This means that if the onshore converters (VSC01 and VSC02) are the ones selected to control the DC power flow in Fig. 11, they should use their DC voltage control schemes (i.e. *UdcCtrl*) for allowing to the PCI to modify their DC voltage references through the droop line tracking method as described in [23]. Likewise, the PCI allows us to define several types of DC voltage control strategies (e.g. master–slave, single slope droop or even multi-slope droop DC voltage control) in order to manage the DC power flow in a multi-terminal or in a PtP-VSC-HVDC network. Nevertheless, the simulations developed in this work for the multi-terminal operation of the *expandable* PtP-VSC-HVDC network are exclusively based on the single slope droop (DC voltage) control. This consideration allows simplifying the analysis of the quasi-stationary voltage support, provided by each onshore VSC unit, in Fig. 11. Moreover, this consideration also allows defining a constant value for the η_i factor presented in Section 4.4.

In this connection, the quasi-stationary voltage support of a VSC unit belonging to an MT-VSC-HVDC system is analysed by considering two single slope droops cases. The first case has been defined such that the output power profile of the OWF is identically distributed between the onshore VSC units VSC01 and VSC02. In other words, $\eta = 0.5$ for both onshore VSC units. The second case is defined such that the output power profile of the OWF is distributed in different proportions between the onshore VSC units as presented in Table 2. The different η proportions have been selected to expose the influence of a variable **APG** magnitude in the quasi-stationary voltage support for the different AC network strengths presented in Fig. 11.

7 Simulation results

7.1 PtP operation of the expandable PtP-VSC-HVDC system

The simulation experiments executed for the PtP operation of the (expandable) PtP-VSC-HVDC system are presented in Fig. 12. It is shown in Fig. 12*a* that the VSC01 unit is subjected to a change in its steady-state active power condition at $t = 10$ s. This reduction (from 560 to 50 MW) in the active power transmitted through the VSC units VSC01 and VSC02 induces different reactive power responses as shown on the left side of Figs. 12*b* and *c*. These reactive power responses depend on the RPC mode utilised and the associated AC network strength (impedance levels) in which the

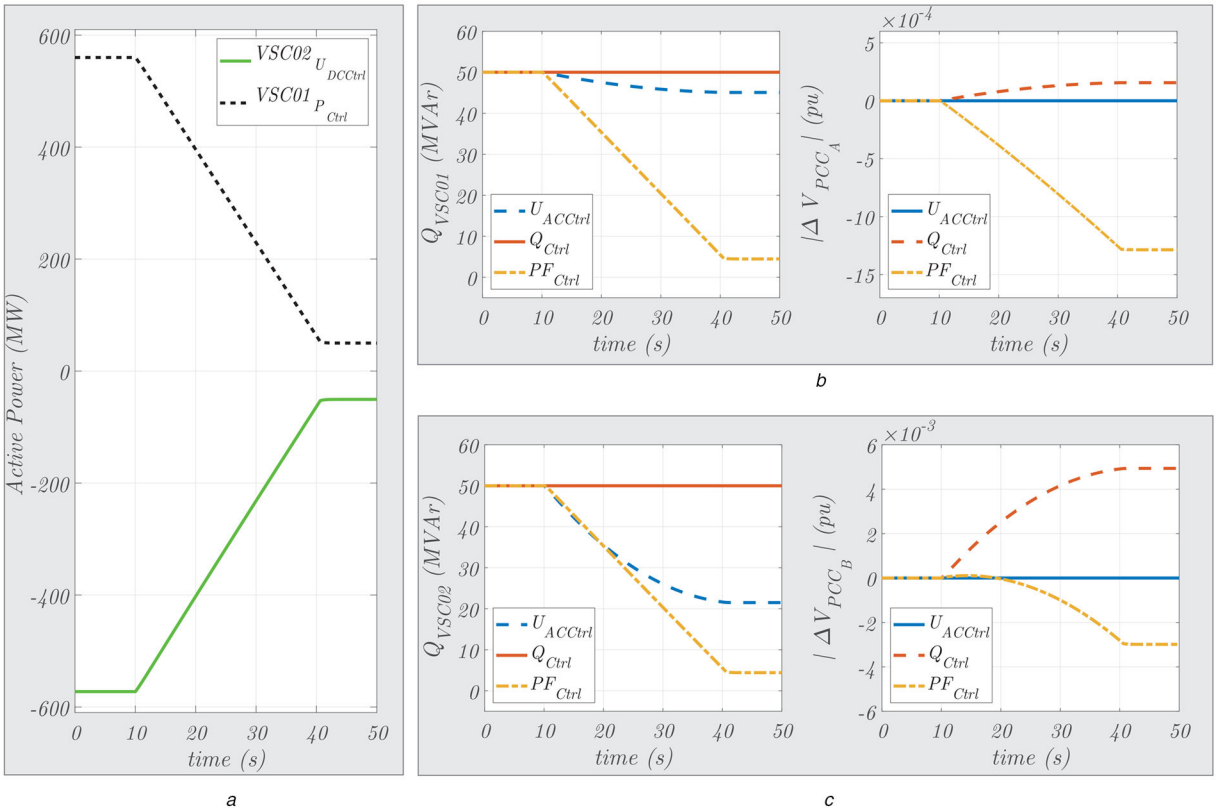

Fig. 12 *Expandable PtP-VSC-HVDC system operating under a PtP-VSC-HVDC network configuration (i.e. the grey elements in Fig. 11 are not connected).* ***(a)*** Linear decrement in the active power transferred through the onshore VSC units, ***(b)*** The left side showing the deployment of the reactive power executed by each RPC mode during the active power decrement and the right side showing the corresponding quasi-stationary voltage deviation experienced by V_{PCC_A} (i.e., ΔV_{PCC_A}) in Fig. 11, ***(c)*** The left side showing the deployment of the reactive power executed by each RPC mode during the active power decrement and the right side showing the corresponding quasi-stationary voltage deviation experienced by V_{PCC_B} (i.e., ΔV_{PCC_B}) in Fig. 11

VSC units are connected to. As described in (7), the PF_{Ctrl} leads to a linear relationship between the **APG** and the **RPG**, which is scaled up by the steady-state power ration factor, $\lambda = 50\,\text{MVAr}/560\,\text{MW}$. Additionally, the deployment of the reactive power executed by the U_{ACCtrl} mode of VSC01 in Fig. 12*b* is comparatively smaller to the one produced by the same RPC mode in the VSC02 unit, as shown on the left side of Fig. 12*c*. These reactive power deployments from each VSC unit will guarantee a constant steady-state voltage magnitude for V_{PCC_A} and V_{PCC_B} as shown on the right side of Figs. 12*b* and *c*, respectively. This non-voltage deviation presented on the right side of Figs. 12*b* and *c* (for the ΔV_{PCC} responses) is completely aligned with the implications observed when projecting the vector field of the **PRR** (described in Section 4.1) over the *PQ* diagrams, as shown in Fig. 7. That is to say, the faster reactive power deployment produced by the U_{ACCtrl} mode on, as shown on the left side of Fig. 12*c* is a consequence of having a shorter curvature ratio in Fig. 7*b*, in comparison to the one exhibited in Fig. 7*a*. This demonstrates that the reduction of the short-circuit impedance in a power system (caused by the decommissioning of conventional power plants) will lead to an increase the **RPG** capabilities of the VSC units to provide quasi-stationary voltage support at transmission levels.

The deviations of the steady-steady voltages V_{PCC_A} and V_{PCC_B} produced by the Q_{Ctrl} mode and the PF_{Ctrl} mode are also observed on the right side of Figs. 12*b* and *c*. If all the ΔV_{PCC} responses in Figs. 12*b* and *c* are examined, it is clear that the U_{ACCtrl} mode is the one that provides the best quasi-stationary voltage support since it does not generate quasi-stationary (steady-state) voltage deviations (ΔV_{PCC}) in each AC network. However, the second-best alternative for providing quasi-stationary voltage support is determined based on the ΔV_{PCC} deviations produced by the Q_{Ctrl} and the PF_{Ctrl} w.r.t. the one generated by the U_{ACCtrl}. It can be seen on the right side of Fig. 12*b* that the steady-state deviation experienced by the V_{PCC_A} voltage (i.e. ΔV_{PCC_A}) is lower when the Q_{Ctrl} mode is utilised. Conversely, on the right side of Fig. 12*c*, the PF_{Ctrl} is the RPC mode, which generates the smaller steady-state voltage deviation ΔV_{PCC_B}. The difference in these two results can be explained based on two factors: the AC network strength of each network (X_{th_A} and X_{th_B} in Fig. 11) and the P_{oVSC} and Q_{oVSC} conditions of each VSC unit. These two factors are simultaneously considered within the areas presented in Figs. 9*a* and *b*, respectively. Ergo, Fig. 9 represents a way to graphically identify (depending on the AC network strength), the second-best and the last RPC mode option to be considered for providing quasi-stationary voltage support depending on the steady-state power conditions (P_o, Q_o) of the VSC unit analysed. Additionally, Fig. 9 is independent of the variability associated to the **APG** magnitude, which is associated with the type of VSC-HVDC network (point-to-point or multi-terminal) in which the onshore VSC unit can be connected to. This statement will be studied in Section 7.2 by enabling the multi-terminal expansion of the PtP-VSC-HVDC system (used in this simulation experiment) as defined in Section 6.2.

7.2 MT operation of the expandable PtP-VSC-HVDC system (case 1)

The simulation results concerning case 1 presented in Table 2, for the MT-VSC-HVDC operation of the expandable PtP-VSC-HVDC system are presented in Fig. 13. It can be seen in Fig. 13*a* that the wind power profile injected into the VSC-HVDC network by the VSC03 unit (shown in Fig. 11) has been equally distributed between the onshore VSC units, as indicated by the η_{1VSC01} and η_{2VSC02} factors in Table 2. The steady-state power conditions analysed for case 1 are shown in Fig. 13*a*, and on the left side of Fig. 13*b* and Fig. 13, respectively. Concretely, the steady-steady power conditions are $Q_{oVSC01} = 2\,\text{MVAr}$, $P_{oVSC01} = 280\,\text{MW}$,

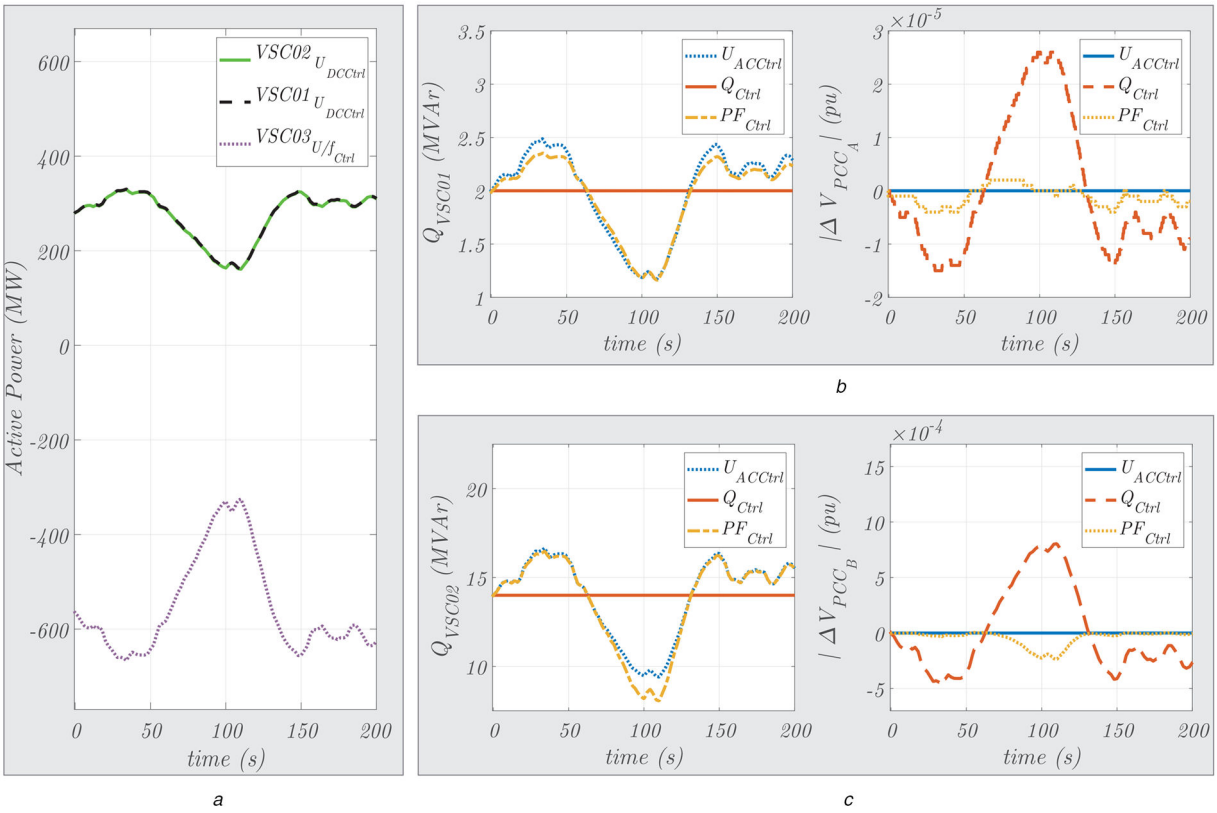

Fig. 13 *Expandable PtP-VSC-HVDC system operating under the MT-VSC-HVDC network configuration shown in Fig. 11.*
(a) Wind power provided by VSC03 and its distribution (in the onshore VSC units) is shown accordingly to case 1 (i.e. ηi description) presented in Table 2, ***(b)*** The left side showing the deployment of the reactive power executed by each RPC mode during the active power decrement and the right side showing the corresponding quasi-stationary voltage deviation experienced by V_{PCC_A} (i.e., ΔV_{PCC_A}) in Fig. 11 **,** ***(c)*** The left side showing the deployment of the reactive power executed by each RPC mode during the active power decrement and the right side showing the corresponding quasi-stationary voltage deviation experienced by V_{PCC_B} (i.e., ΔV_{PCC_B}) in Fig. 11

$Q_{oVSC02} = 14$ MVAr and $P_{oVSC02} \simeq 280$ MW. These steady-state power conditions have been selected to assess the feasibility of enabling the simultaneous operation of the PF_{Ctrl} in the VSC onshore units of the MT-VSC-HVDC network configuration shown in Fig. 11.

In the left side of Figs. 13*b* and *c*, the reactive power deployments of each onshore VSC unit are shown. It can be seen on the left side of Figs. 13*b* and *c* that the deployments of the reactive power executed by the PF_{Ctrl} and the U_{ACCtrl} are quite similar. These reactive power similarities also derive in smaller quasi-stationary voltage deviations (ΔV_{PCC} responses) as the ones presented on the right side of Figs. 13*b* and *c*. In other words, the PF_{Ctrl} exhibits for both onshore VSC units a higher level of quasi-stationary voltage support (less ΔV_{PCC} deviation), if it is compared against the ΔV_{PCC} deviations generated by the Q_{Ctrl} mode observed on the right side of Figs. 13*b* and *c*. However, it is relevant to clarify that for this case, the steady-state power ratio of VSC01 is $\lambda_{VSC01} = 0.007$ MVAr/MW. This means that the corresponding reference of the PF_{Ctrl} (i.e. PF^* in Fig. 3) for VSC01 is, respectively, $PF^*_{VSC01} = 0.9999$. In other words, the feasibility of using the PF_{Ctrl} mode in a VSC unit connected to a low impedance network (e.g. X_{th_A} in Fig. 11) would require, a high precision measurement system to consider (at least) a four decimals resolution for the PF_{Ctrl} mode. This high precision measurement requirement and the level of quasi-stationary voltage support achieved by the PF_{Ctrl} in Fig. 13*b* makes impractical its implementation for a low impedance network.

On the other hand, the steady-state power ratio associated to the VSC02 unit is $\lambda_{VSC02} = 0.05$ MVAr/MW. This means that the PF_{Ctrl} reference for VSC02 is, respectively, $PF^*_{VSC02} = 0.9987$. Thus, it can be seen that the increment in the impedance network (e.g. X_{th_B} in Fig. 11) can lead to a slightly less precise (or more flexible) resolution for the utilisation of the PF_{Ctrl} mode. However, the utilisation of the PF_{Ctrl} mode will just lead into superior quasi-stationary voltage support if it is compared against the one provided by the Q_{Ctrl} mode as shown in this simulation experiment. Thus, the quasi-stationary voltage support information presented in Fig. 9 have been verified considering, an identical distribution of the wind power, between the onshore VSC units of the expandable PtP-VSC-HVDC system operating under an MT-VSC-HVDC network configuration.

7.3 MT operation of the expandable PtP-VSC-HVDC system (case 2)

The simulation results concerning case 2 presented in Table 2 for the MT-VSC-HVDC operation of the expandable PtP-VSC-HVDC system are presented in Fig. 14. In Fig. 14*a*, it can be seen that the wind power profile provided by the VSC03 unit, has been unequally distributed between the onshore VSC units. This unequal DC power distribution is due to the fact that the PCI has set a different DC voltage set-point (cf. Section 6.2) for each onshore station w.r.t. the ones used for the previous multi-terminal operation analysis (case 1). As shown in Fig. 14*a*, almost the entire wind profile ($\eta_{2_{VSC02}} \simeq 0.98$) is been captured by the VSC02 unit. This means that most of the wind power will be provided to the high impedance network X_{th_B} (as shown in Fig. 11). Accordingly to Fig. 9*b*, the selection of the PF_{Ctrl} as the second-best option for providing quasi-stationary voltage support in a high impedance network, is slightly more suitable than in a low impedance network condition (Fig. 9*a*). Thus, if the steady-state reactive power conditions are examined on the left side of Figs. 14*b* and *c* (i.e. $Q_{oVSC01} = Q_{oVSC02} = 70$ MVAr), the steady-stated power ratios can be determined: $\lambda_{VSC01} = 4.441$ MVAr/MW and $\lambda_{VSC02} = 0.111$ MVAr/MW. These steady-stated power ratios automatically define the references utilised for the PF_{Ctrl} in each VSC onshore unit, that is to say $PF^*_{VSC01} = 0.2197$ and

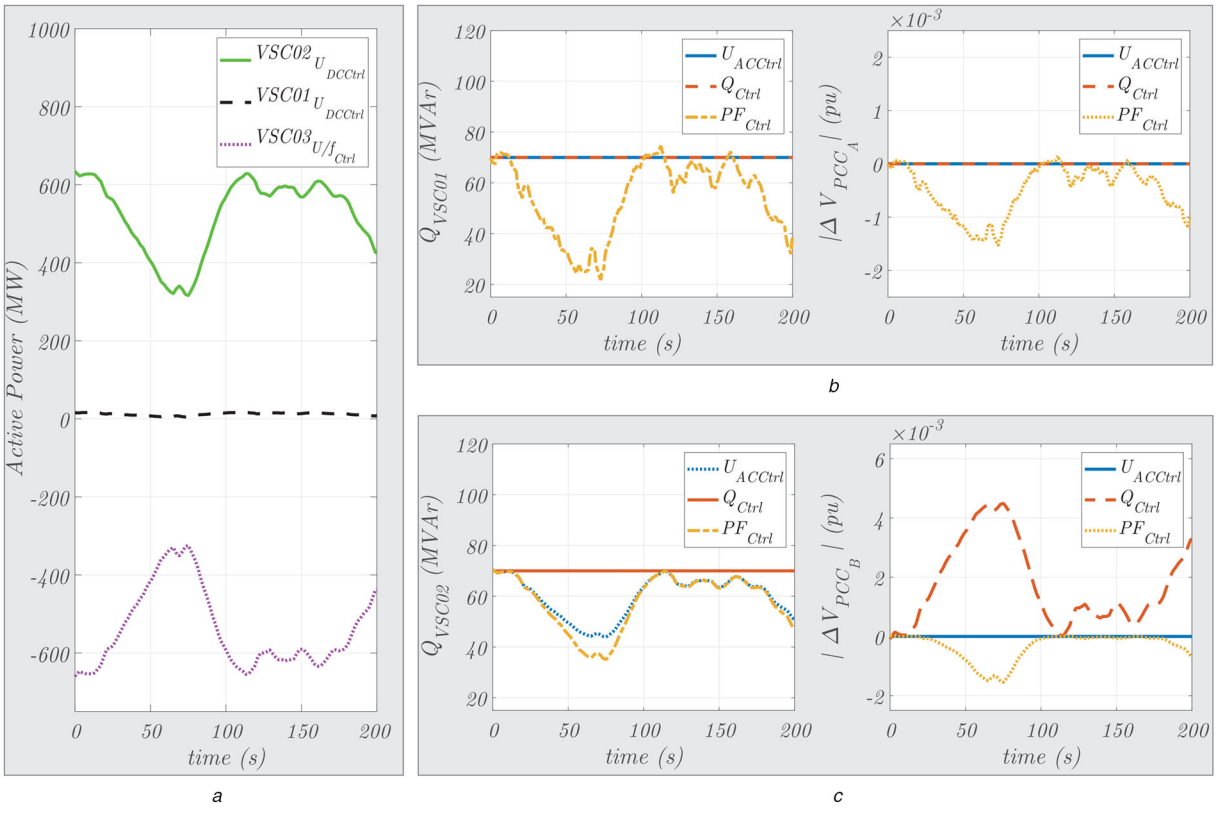

Fig. 14 *Expandable PtP-VSC-HVDC system operating under the MT-VSC-HVDC network configuration shown in Fig. 11.*
(a) Wind power provided by VSC03 and its distribution (in the onshore VSC units) is shown accordingly to case 2 (i.e. ηi description) presented in Table 2, ***(b)*** The left side showing the deployment of the reactive power executed by each RPC mode during the active power decrement and the right side showing the corresponding quasi-stationary voltage deviation experienced by V_{PCC_A} (i.e., $\Delta V_{\mathrm{PCC}_A}$) in Fig. 11, ***(c)*** The left side showing the deployment of the reactive power executed by each RPC mode during the active power decrement and the right side showing the corresponding quasi-stationary voltage deviation experienced by V_{PCC_B} (i.e., $\Delta V_{\mathrm{PCC}_B}$) in Fig. 11

$\mathrm{PF}^{*}_{\mathrm{VSC02}} = 0.9939$. Then, if the reactive power deployment for each RPC is observed on the left side of Fig. 14*b*, it is found that the Q_{Ctrl} and the $\mathrm{AC}_{\mathrm{Ctrl}}$ exhibit almost an identical behaviour. This means that the steady-state power conditions considered for the VSC01 unit and its AC network strength value (i.e. X_{th_B} in Fig. 11) generate a $\gamma_{Q_{\mathrm{Ctrl}}} \simeq (\pi/2)$ as indicated in Section 4.4. Consequently, the quasi-stationary voltage deviation (i.e. $\Delta V_{\mathrm{PCC}_A}$) induced by the $\mathrm{PF}_{\mathrm{Ctrl}}$ is comparatively higher w.r.t. the ones produced by other RPC modes as shown on the right side of Fig. 14*b*. The deviation induced by the $\mathrm{PF}_{\mathrm{Ctrl}}$ is an expected result since, it depends on the λ_{VSC01} value selection as explained in Sections 4.3 and 4.4.

The quasi-stationary voltage deviations of V_{PCC} in the AC network *B* (i.e. $\Delta V_{\mathrm{PCC}_B}$) associated to the different reactive power modulation executed by each RPC mode in the VSC02 unit, are shown on the right side of Fig. 14*c*. Here, it is shown that the utilisation of the Q_{Ctrl} mode leads to the worst quasi-stationary voltage support if it is compared against the other RPC modes. These results demonstrate that the regions obtained in Fig. 9 (based on the DDBM analysis), can effectively classify the level of quasi-stationary voltage support provided by each RPC mode in a single-infeed VSC unit independently of the **APG** characteristics (i.e. variable of constant) associated to the VSC-HVDC network configuration. Additionally, it can be seen that the influence of the unequal wind power distribution (between the onshore VSC units) over the quasi-stationary voltage support level, is again determined, by mainly two factors. First, the evolution of the power-trajectories associated to each RPC mode and second, the steady-state power conditions in which the Q_{Ctrl} and the $\mathrm{PF}_{\mathrm{Ctrl}}$ operate under different AC network strength levels.

8 Conclusion

This paper presents an analytical method based on directional derivatives to assess the level of quasi-stationary voltage support provided by a single-infeed VSC unit operating within a point-to-point or a multi-terminal VSC-HVDC system. The assessment was performed by proposing a set of mathematical formulations for describing the active power control and RPC modes, during the quasi-stationary operation of a VSC unit. The formulations proposed allowed to define dynamic vectors, which were used to separately analyse the control actions of a VSC unit and the AC network features (i.e. AC network strength) of a reduced power system representation. The analysis of the interaction of the dynamic vectors led to defining an IVSF, which provides the necessary geometrical insight to determine the power-trajectories for each RPC mode considered. The determination of these power-trajectories allowed us to develop a quantitative criteria based on Riemann's sums (S factors) and Euclidean distances. This quantitative criterion produced a graphical representation in which the conditions defining the first, the second and the third-best RPC option for providing quasi-stationary voltage support (under different AC network strength conditions) were obtained.

The graphical representation was derived by implementing a MATLAB code in which symmetrical regions were obtained and projected over the PQ diagram of the VSC unit. These projections facilitate the assessment of the level of quasi-stationary voltage support provided by each RPC mode, as a function of the AC network strength and the steady-state power conditions associated with the VSC unit. It was revealed that in some cases, the power factor control ($\mathrm{PF}_{\mathrm{Ctrl}}$) could lead to better quasi-stationary voltage support if it is compared against the RPC (Q_{Ctrl}) under the same high impedance network and the same (and very specific) steady-state power conditions. Additionally, it was also discussed that the implementation of such RPC mode (i.e. $\mathrm{PF}_{\mathrm{Ctrl}}$) in a VSC unit might result in very challenging due to its high precision measurement requirements. These conclusions were verified by performing simulation experiments in DIgSILENT PowerFactory 2018 by considering an expandable point-to-point VSC-HVDC system operating in a multi-terminal and a point-to-point configuration. The different VSC-HVDC network configurations analysed

revealed that the influence of the **APG** over the quasi-stationary voltage support is modulated by mainly two factors: the evolution of the power-trajectories associated to each RPC mode and, the steady-state power conditions in which the Q_{Ctrl} and the PF_{Ctrl} operate for different AC network impedance levels. The proposed DDBM represents a valuable tool to assist transmission systems operators and VSC units manufacturers to estimate the expected speed of the reactive power deployment that would be required in new VSC units installations, as a function of the decrement of the short-circuit power levels in the power system (a real-world problem) caused by the massive integration of renewable energy systems. Additionally, the estimation of the RPG's evolution attributed to each RPC mode is a necessary step during the coordination studies (interaction analysis) of VSC units with other voltage support elements like the transformer tap-changers, which operates within the same quasi-stationary voltage time-frame considered in this paper. These coordination studies will be covered in a future publication.

9 Acknowledgment

This research was executed in cooperation with Energinet.dk and TenneT TSO B.V under the COBRAcable project and co-financed by the European Commission under the European Energy Program for Recovery. It is a joint project of Aalborg University and the Delft University of Technology. The authors also thank Abraham Vivas (Polytechnic University of Cartagena) for the insightful discussions on the developed Python and MATLAB codes for automated calculations and art works.

10 References

[1] Coronado, L., Longas, C., Rivas, R., *et al.*: 'INELFE: main description and operational experience over three years in service'. AEIT HVDC Int. Conf. (AEIT HVDC), Florence, Italy, 2019, pp. 1–6

[2] Barnes, M., Van Hertem, D., Teeuwsen, S.P., *et al.*: 'HVDC systems in smart grids', *Proc. IEEE*, 2017, **105**, (11), pp. 2082–2098

[3] Tourgoutian, B., Alefragkis, A.: 'Design considerations for the cobracable HVDC interconnector'. IET Int. Conf. on Resilience of Transmission and Distribution Networks (RTDN 2017), Birmingham, UK, 2017, pp. 1–7

[4] Mehrjerdi, H., Ghahremani, E., Lefebvre, S., *et al.*: 'Authenticated voltage control of partitioned power networks with optimal allocation of STATCOM using heuristic algorithm', *IET Gener. Transm. Distrib.*, 2013, **7**, (9), pp. 1037–1045

[5] Mehrjerdi, H., Lefebvre, S., Saad, M., *et al.*: 'Coordinated control strategy considering effect of neighborhood compensation for voltage improvement in transmission systems', *IEEE Trans. Power Syst.*, 2013, **28**, (4), pp. 4507–4515

[6] Cai, L., Erlich, I.: 'Power system static voltage stability analysis considering all active and reactive power controls – singular value approach'. IEEE Lausanne Power Tech, 2007, pp. 367–373

[7] Urquidez, O.A., Xie, L.: 'Singular value sensitivity based optimal control of embedded VSC-HVDC for steady-state voltage stability enhancement', *IEEE Trans. Power Syst.*, 2016, **31**, (1), pp. 216–225

[8] Zeni, L., Jóhannsson, H., Hansen, A.D., *et al.*: 'Influence of current limitation on voltage stability with voltage sourced converter HVDC'. IEEE PES ISGT Europe 2013, Lyngby, Denmark, 2013, pp. 1–5

[9] Zhao, C., Yuan, B., Xu, J.: 'Active power and AC voltage slope control for VSC connected to ac system with low SCR'. 12th IET Int. Conf. on AC and DC Power Transmission (ACDC 2016), Beijing, China, 2016, pp. 1–6

[10] Zhao, C., Li, L., Li, G., *et al.*: 'A novel coordinated control strategy for improving the stability of frequency and voltage based on VSC-HVDC'. Third Int. Conf. on Electric Utility Deregulation and Restructuring and Power Technologies, Nanjing, China, 2008, pp. 2202–2206

[11] Erlich, I., Shewarega, F., Winter, W.: 'A method for incorporating VSC-HVDC into the overall grid voltage-reactive power control task'. 2016 Power Systems Computation Conf. (PSCC), Genoa, Italy, 2016, pp. 1–7

[12] Perilla, A., Torres, J.L.R., van der Meijden, M.A.M.M., *et al.*: 'Analysis of a power factor regulation strategy for an embedded point-to-point MMC-HVDC system'. 2018 IEEE Int. Energy Conf. (ENERGYCON), Limassol, Cyprus, 2018, pp. 1–6

[13] European Commission: 'ENTSO-E network code on requirements for grid connection of high voltage direct current systems and direct current-connected power park modules', Official Journal of the European Union, 2016

[14] Wachal, R., Jindal, A., Dennetiere, S.: 'Guide for the development of models for HVDC converters in a HVDC grid', CIGRE, 2014

[15] Kraiczy, M., Stetz, T., Braun, M.: 'Parallel operation of transformers with on load tap changer and photovoltaic systems with reactive power control', *IEEE Trans. Smart Grid*, 2018, **9**, (6), pp. 6419–6428

[16] Van Pham, H., Rueda, J.L., Erlich, I.: 'Probabilistic evaluation of voltage and reactive power control methods of wind generators in distribution networks', *IET Renew. Power Gener.*, 2015, **9**, (3), pp. 195–206

[17] Aik, D.L.H., Andersson, G.: 'Fundamental analysis of voltage and power stability of single-infeed voltage-source converter HVDC systems', *IEEE Trans. Power Deliv.*, 2019, **34**, (1), pp. 365–375

[18] Irnawan, R., Perilla, A., Da Silva, F.F., *et al.*: 'Preparing the expansion of a point-to-point VSC link into a multi-terminal HVDC transmission system: the COBRAcable research project'. CIGRE Symp., Aalborg, Denmark, 2019

[19] Kirby, N.: 'Current trends in DC: voltage-source converters', *IEEE Power Energy Mag.*, 2019, **17**, (3), pp. 32–37

[20] Saad, H., Peralta, J., Dennetière, S., *et al.*: 'Dynamic averaged and simplified models for MMC-based HVDC transmission systems', *IEEE Trans. Power Deliv.*, 2013, **28**, (3), pp. 1723–1730

[21] Zhao, M., Yuan, X., Hu, J., *et al.*: 'Voltage dynamics of current control time-scale in a VSC-connected weak grid', *IEEE Trans. Power Syst.*, 2016, **31**, (4), pp. 2925–2937

[22] Rault, P., Despouys, O., Petit, A., *et al.*: 'Implementation of a dedicated control to limit adverse interaction in multi-vendor HVDC systems'. 15th IET Int. Conf. on AC and DC Power Transmission (ACDC 2019), Boston, MA, USA, 2019, pp. 1–6

[23] Irnawan, R.: '*Planning and control of expandable multi-terminal VSC-HVDC transmission systems*' (Springer, Basel, Switzerland, 2020, 1st edn.)

[24] Saad, H., Dennetière, S., Mahseredjian, J., *et al.*: 'Modular multilevel converter models for electromagnetic transients', *IEEE Trans. Power Deliv.*, 2014, **29**, (3), pp. 1481–1489

[25] Abdalrahman, A., Isabegovic, E.: 'Dolwin1 – challenges of connecting offshore wind farms'. 2016 IEEE Int. Energy Conf. (ENERGYCON), Leuven, Belgium, 2016, pp. 1–10

[26] Rueda Torres, J.L., Korai, A., Cepeda, J.C., *et al.*: 'Implementation of simplified models of DFIG-based wind turbines for RMS-type simulation in DIgSILENT PowerFactory', in Rueda Torres, J.L. (Ed.): '*Powerfactory applications for power system analysis*' (Springer International Publishing, Switzerland, 2014), pp. 197–220

[27] 'Energinet. Electricity balance data'. Available at https://www.energidataservice.dk/en/dataset/electricityprodex5minrealtime, accessed December 2019